

Analysis of performance of three- and five-stack achromatic half-wave plates at millimeter wavelengths

Tomotake Matsumura

*School of Physics and Astronomy
University of Minnesota, Twin Cities
116 Church St. SE, Minneapolis, Minnesota, 55455*

tmatsumu@physics.umn.edu

*Current address: California Institute of Technology
1200 E. California Blvd. Mail Code 59-33 Pasadena, CA 91125*

tm@caltech.edu

Shaul Hanany

*School of Physics and Astronomy
University of Minnesota, Twin Cities
116 Church St. SE, Minneapolis, Minnesota, 55455*

hanany@physics.umn.edu

Bradley R. Johnson

*Department of Astrophysics
University of Oxford
Keble Road Oxford OX1 3RH England, UK*

bjohnson@physics.ox.ac.uk

Terry J. Jones

*School of Physics and Astronomy
University of Minnesota, Twin Cities
116 Church St. SE, Minneapolis, Minnesota, 55455*

tjj@astro.umn.edu

Prashanth Jonnalagadda

*Department of Computer Science and Engineering
University of Minnesota, Twin Cities
200 Union Street SE, Minneapolis, Minnesota, 55455
jonn0006@umn.edu*

We study the performance of achromatic half-wave plates (AHWP) as a function of their construction parameters, the detection bandwidth of a power detector operating in the millimeter wave band, and the spectral shape of the incident radiation. We focus particular attention on the extraction of the degree of incident polarization and its orientation angle from the intensity measured as a function of AHWP rotation angle, which we call the IVA (intensity versus angle). We quantify the phase offset of the IVA and point to potential systematic errors in the extraction of this offset in cases where the incident spectrum is not sufficiently well known. We show how the phase offset and modulation efficiency of the AHWP depend on the relative angles between the plates in the stack and find that high modulation efficiency can be achieved with alignment accuracy of few degrees.

© 2018 Optical Society of America

OCIS codes: 000.0000, 999.9999.

1. Introduction

Recent experimental efforts in observational cosmology have been focused on searching for a signature from an inflationary period that occurred a short instant after the big bang. This signature is predicted to be imprinted in the polarization of the cosmic microwave background (CMB) radiation. Inflation predicts an inflationary gravitational-wave background (IGB) that left a particular pattern of linear polarization on the CMB. This pattern is different from that originating from primordial density anisotropy, which is the main source for the spatial intensity fluctuations over the sky and for a different, stronger linear polarization pattern. In the past few years, several groups have started to characterize the polarization signal coming from the primordial density anisotropy.^{1,2} The polarization pattern from the IGB is expected to be at least an order of magnitude smaller and it has not been detected yet.

Thorough understanding of foregrounds and good control of systematic errors will be required to extract the small signal from the IGB. Both requirements lead to polarimeter designs that implement broad frequency coverage. Examples of such polarimeters are EBEX,

a NASA supported balloon-borne experiment³ that is being constructed by the authors of this paper and their collaborators, BICEP/SPUD, CLOVER, QUIET, SPIDER, PAPP, and PolarBear.⁴⁻⁹

A common technique to measure linearly polarized radiation is to use a rotating half-wave plate (HWP) together with a linear polarizer. The technique has been used extensively in the optical and IR wavelengths.¹⁰⁻¹³ The first experiment to report CMB polarization results with this technique was MAXIPOL.^{14,15} Although a HWP is a device that operates over narrow band of frequencies there are standard techniques to construct an 'achromatic HWP' (AHWP) that operates over a much broader range.¹⁶⁻²⁰ An AHWP is a stack of birefringent plates that are aligned with specific relative orientation angles between their optic axes. With an appropriate choice of angles it is possible to achieve modulation efficiency that is close to 100 % over a large fraction of the millimeter wavelength band.²⁰

The linear polarization content of incident radiation can be characterized in terms of two parameters, the degree of polarization P_{in} and the orientation angle α_{in} . An equivalent set is the normalized Stokes parameters Q_{in}/I_{in} and U_{in}/I_{in} (see Section 2 for a definition). To reconstruct these parameters from the signal detected by the instrument it is essential to quantify the extent to which the polarimeter itself changes the input parameters.

In this paper, we present a computational study of the effects introduced by three- or five-stack AHWPs that are designed to fit CMB polarimeters operating in the range 120 – 480 GHz. This work is motivated by EBEX that will implement a rotating 5-stack AHWP to search for the faint signals from the IGB. In Sections 2 and 3 we describe the mathematical formalism and define the figures of merit that are used to reconstruct the state of incident polarized light from the measured intensity. In Section 4 we use the figures of merit to quantify how well the incident polarization can be reconstructed. Section 5 discusses effects that arise from uncertainties in the spectrum of the incident radiation. In Section 6 we assess the performance of an AHWP as a function of its construction parameters. A summary of the key conclusions is given in Section 7.

2. Polarimeter Model

We consider a polarimeter that consists of an AHWP that rotates at a frequency f_0 , a linear polarizer, and a power detector (e.g. a bolometer), as shown in Figure 1. The angle ρ gives the rotation angle of the AHWP around its axis of symmetry z . In such a polarimeter information about the incident polarization is contained in the intensity that is detected by the detector as a function of ρ . To a good approximation the detected intensity is sinusoidal as a function of ρ with a frequency of $4f_0$ when there is a high signal-to-noise ratio. Our primary interest in this paper is to analyze the detected intensity as a function of ρ , which we call IVA (intensity vs. angle), with the purpose of reconstructing the incident polarization.

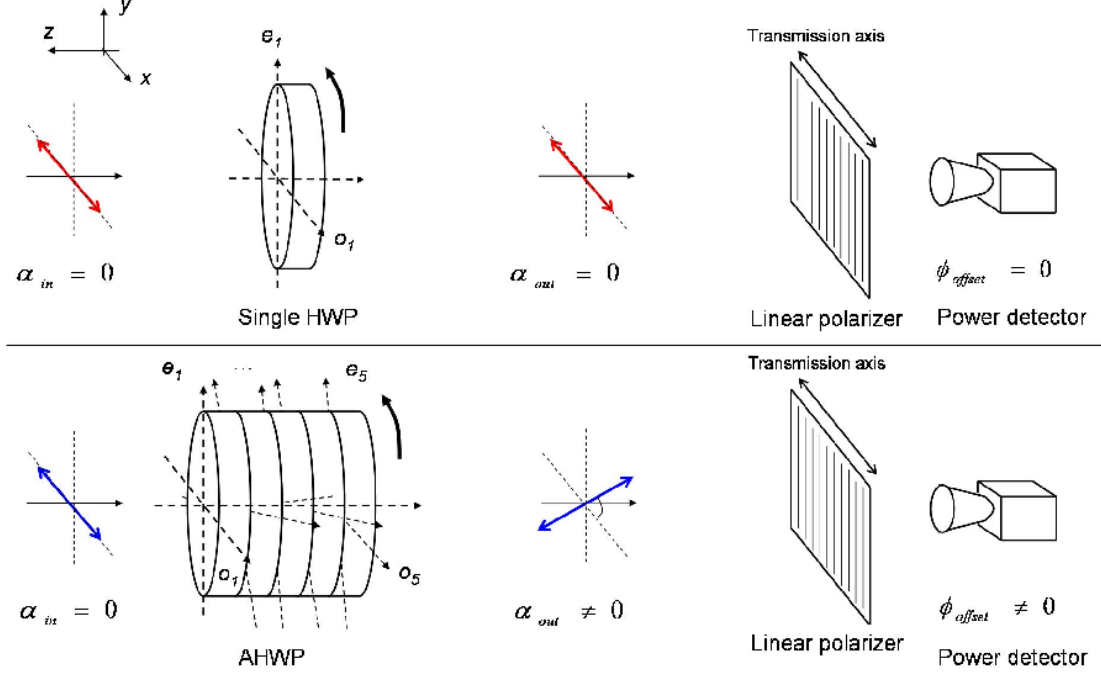


Fig. 1. A schematic diagram of the HWP polarimeter model. The transmission axis of a linear polarizer is parallel to the x axis.

We use Mueller matrices to describe the signal in the approximation of normal incidence on the WP. We neglect the effect of absorption by the wave plate or effects of reflections between media that have different indices of refraction.

Consider an input Stokes vector \vec{S}_{in} of radiation propagating along the z axis that is incident on the polarimeter. The Stokes vector incident on the detector, which we call the output Stokes vector, is

$$\vec{S}_{out} = G \prod_{i=1}^m [R(-\rho - \theta_i) \Gamma_i(\Delta\delta) R(\rho + \theta_i)] \vec{S}_{in}(\alpha_{in}, P_{in}), \quad (1)$$

where

$$\Delta\delta = 2\pi \frac{\nu}{c} |n_o - n_e| d, \quad (2)$$

$$\begin{aligned} \vec{S}_{in} &= (I_{in}, Q_{in}, U_{in}, 0) \\ &= I(\nu)(1, P_{in} \cos 2\alpha_{in}, P_{in} \sin 2\alpha_{in}, 0), \end{aligned} \quad (3)$$

G is the Mueller matrix of the linear polarizer, R is a rotation matrix, Γ is the Mueller matrix of a retarder, and \vec{S}_{in} is the Stokes vector of the incident radiation, which is a function of the polarization angle α_{in} and of the degree of polarization P_{in} . Information about the spectrum of the incident radiation is contained in $I(\nu)$. We initially assume that the intensity of the

incident radiation is constant with frequency, $I(\nu) = I_0 = \text{const}$. We discuss the effects of a non-constant incident spectrum in Section 5. Equation 1 assumes m wave plates in the stack; in this paper $m = 1, 3$ or 5 . The variable $\Delta\delta$ is the retardance of a single wave plate and is a function of the ordinary and extraordinary indices of refraction n_o and n_e , respectively, the thickness of a single wave plate d , and the electromagnetic frequency of light ν . Throughout this paper, we assume that the incident radiation is not circularly polarized. We also assume that α_{in} and P_{in} are independent of ν . The components of the Mueller matrices are

$$\Gamma(\Delta\delta) = \begin{bmatrix} 1 & 0 & 0 & 0 \\ 0 & 1 & 0 & 0 \\ 0 & 0 & \cos \Delta\delta & -\sin \Delta\delta \\ 0 & 0 & \sin \Delta\delta & \cos \Delta\delta \end{bmatrix}, \quad (4)$$

$$R(\theta) = \begin{bmatrix} 1 & 0 & 0 & 0 \\ 0 & \cos 2\theta & -\sin 2\theta & 0 \\ 0 & \sin 2\theta & \cos 2\theta & 0 \\ 0 & 0 & 0 & 1 \end{bmatrix}, \quad (5)$$

and

$$G = \frac{1}{2} \begin{bmatrix} 1 & 1 & 0 & 0 \\ 1 & 1 & 0 & 0 \\ 0 & 0 & 0 & 0 \\ 0 & 0 & 0 & 0 \end{bmatrix}. \quad (6)$$

As shown in Figure 1, we choose the transmission axis of the ideal linear polarizer to be aligned with the $+x$ axis. We define all the angles of rotation about the z axis with respect to the transmission axis of the grid. According to the usual convention, angles increase in the counter-clockwise direction from the $+x$ axis in the xy plane. The relative orientation of plate $i = 2, 3, \dots$ in the stack relative to the first plate is given by θ_i . The ordinary axis of the first plate is aligned with the x axis when $\rho = 0$ degrees. We use the notation $\vec{\theta}$ to denote the entire set of relative orientation angles.

The output of the detector is a function of its detection bandwidth and the intensity term of \vec{S}_{out} . We assume that the detector has top-hat response of width $\Delta\nu$ about a center frequency ν_c . Note that the limit $\Delta\nu \rightarrow 0$ is equivalent to the case of illuminating the polarimeter with monochromatic light. With these assumptions the first element of the output Stokes vector can be written as

$$\langle I_{out} \rangle(\nu_c, \Delta\nu, \alpha_{in}, P_{in}, \vec{\theta}, \rho) = \int_{\nu_c - \frac{\Delta\nu}{2}}^{\nu_c + \frac{\Delta\nu}{2}} I_{out}(\nu, \alpha_{in}, P_{in}, \vec{\theta}, \rho) d\nu. \quad (7)$$

A plot of $\langle I_{out} \rangle$ as a function of ρ is the IVA. (Throughout this paper angle brackets $\langle \rangle$ denote integration over frequency.) For a single HWP I_{out} of Equation 7 is

$$I_{out}(\nu) = \frac{I_0}{2} \left(1 + P_{in} \cos 2\alpha_{in} \cos^2 \frac{\Delta\delta(\nu)}{2} + P_{in} \sin^2 \frac{\Delta\delta(\nu)}{2} \cos(4\rho - 2\alpha_{in}) \right) \quad (8)$$

and an analytic integration over any bandwidth is straight forward. For a three- and five-stack AHWP the analytic expressions are more complicated.

It is the goal of this paper to discuss quantitatively how the amplitude and phase of the IVA depend on the construction parameters of the AHWP. Specifically, we make a quantitative mapping between the measured amplitude and phase of the IVA and the two parameters characterizing the incident polarization, the degree of input polarization P_{in} and its orientation angle α_{in} .

When there is a finite detection bandwidth $\Delta\nu \neq 0$ the amplitude and phase of the IVA are calculated in the following way. We calculate the intensities as a function of angle ρ for each frequency within the bandwidth. We then sum the calculated intensities angle by angle to obtain a final IVA. The amplitude and phase are determined from that IVA.

All of the analysis in this paper is computational. IVAs have been calculated as a function of various parameters of the incident radiation and of the construction of the HWP. Many of the results were calculated by two independent computer codes to check for errors. Where practical, the results were compared to analytical calculations and agreement has been verified.

3. Figures of Merit

Figure 2 shows the IVA for the case of a single sapphire HWP and for an AHWP made of a stack of three and five sapphire plates. Table 1 lists the parameters of the plates used to generate these IVAs. The thickness of each wave plate gives $\Delta\delta = \pi$ when $\nu_{WP} = 300$ GHz. The top panels in Figure 2 show the IVA for a monochromatic detection bandwidth ($\Delta\nu = 0$). In the panels on the bottom the detection bandwidth is $\Delta\nu = 60$ GHz. The incident light is polarized parallel to the transmission axis of the grid, $\alpha_{in} = 0$ degrees.

Several generic features are apparent. The reduction in the amplitude of the IVA with a single HWP (left column) is a consequence of its chromaticity. Linear input polarization becomes elliptical when it passes through a wave plate that is optimized for a different frequency. There is substantially smaller reduction in amplitude of modulation for the 3-stack (middle column) or 5-stack (right column). However, whereas for a single plate the phase of the IVA is the same between different frequencies, or with a broad detection bandwidth, it becomes a function of frequency for the case of an AHWP. We define the phase angle ϕ of the IVA as

$$\langle I_{out} \rangle = A_0 + A_4 \cos(4\rho - 4\phi), \quad (9)$$

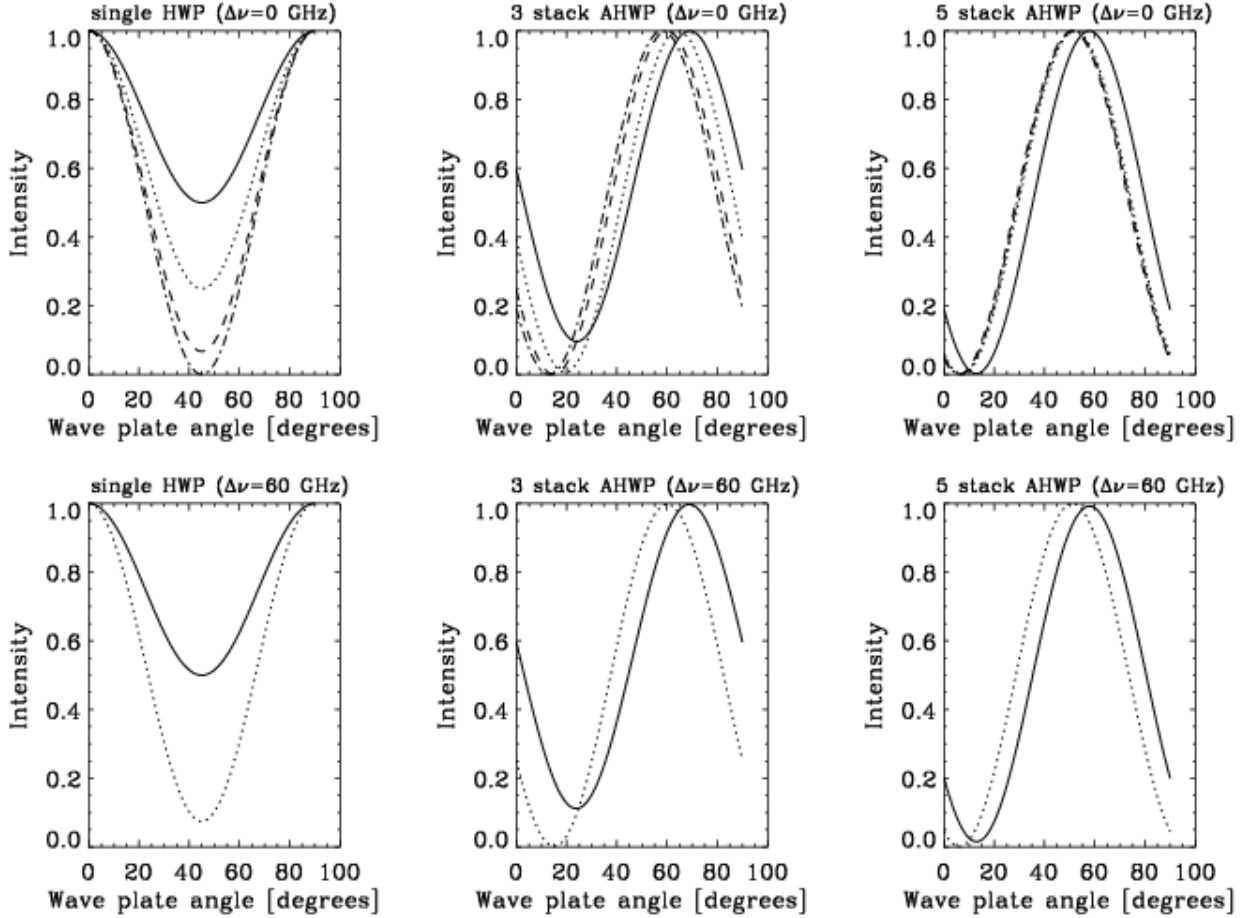


Fig. 2. IVA for monochromatic light (top panels) and for broadband radiation (bottom panels) for a single HWP, a three-stack AHWP, and a five-stack AHWP (left to right). See Table 1 for the parameters of the plates and for the details about the simulations used for the calculations. Frequencies of 150 (solid), 200 (dash), 250 (dot), 300 (dash-dot) GHz are used for the case of monochromatic light. For the broadband case we use 150 ± 30 GHz (solid) and 250 ± 30 GHz (dot). In all the panels, the maximum intensity is normalized to 1.

where A_0 and A_4 denote the average level and the modulation amplitude of the IVA, respectively. For the case of a single HWP the forms of A_0 and A_4 are

$$A_0 = \frac{I_0}{2} \left(\Delta\nu + P_{in} \cos 2\alpha_{in} \int_{\nu_c - \frac{\Delta\nu}{2}}^{\nu_c + \frac{\Delta\nu}{2}} \cos^2 \frac{\Delta\delta(\nu)}{2} d\nu \right), \quad (10)$$

and

$$A_4 = \frac{I_0 P_{in}}{2} \int_{\nu_c - \frac{\Delta\nu}{2}}^{\nu_c + \frac{\Delta\nu}{2}} \sin^2 \frac{\Delta\delta(\nu)}{2} d\nu. \quad (11)$$

From a comparison of Equations 8 and 9 it is evident that in this case $\phi = \alpha_{in}/2$ and that it is independent of frequency. Since we chose $\alpha_{in} = 0$ degrees for the simulation shown in the left panels of Figure 2, $\phi = 0$ degrees. However, for an AHWP the phase ϕ is a

Incident intensity	$I = 1$
Indices of refraction of sapphire ²¹	$n_o = 3.047, n_e = 3.364$
Thickness of each wave plate, d	1.58 mm ($\leftrightarrow \nu_{WP} = 300$ GHz)
Bandwidth of frequency, $\nu_c + \Delta\nu$	150 ± 30 GHz, 250 ± 30 GHz
Orientation angles of three-stack AHWP, $\vec{\theta}_3$	(0, 58, 0) degrees
Orientation angles of five-stack AHWP, $\vec{\theta}_5$	(0, 29, 94.5, 29, 2) degrees
Resolution of frequency	0.5 GHz
Resolution of wave plate angle	0.1 degrees

Table 1. Parameters of the wave plates and parameters used in the simulations to calculate the IVA.

function of the thickness of the HWP, the detection bandwidth and the relative orientation angles. Mathematically $\phi = \phi(\nu_c, \Delta\nu, \alpha_{in}, \vec{\theta})$, and therefore the IVAs in the middle and right columns of Figure 2 show non-zero phase angles. We define this overall 'phase offset' of the 3- and 5-stack AHWPs as ϕ_0 . The quantity ϕ_0 is the value of ϕ when $\alpha_{in} = 0$ degrees (e.g. $\phi_0 \sim 65$ degrees for the solid line of the middle bottom panel of Figure 2).

A useful figure of merit for the operation of a polarimeter is the 'modulation efficiency'¹⁹ defined as

$$\epsilon = \epsilon(\nu_c, \Delta\nu, \alpha_{in}, P_{in}, \vec{\theta}) = \frac{P_{out}}{P_{in}}. \quad (12)$$

The efficiency ϵ is a measure of the de-polarization introduced by the polarimeter and is an essential element in reconstructing the incident polarization P_{in} from the one measured by the experiment P_{out} . In this paper we calculate ϵ by extracting P_{out} from the IVA. P_{out} is calculated from the ratio,

$$P_{out} = P_{out}(\nu_c, \Delta\nu, \alpha_{in}, P_{in}, \vec{\theta}) = \frac{\langle I_{out} \rangle_{max} - \langle I_{out} \rangle_{min}}{\langle I_{out} \rangle_{max} + \langle I_{out} \rangle_{min}}. \quad (13)$$

Here $\langle I_{out} \rangle_{max}$ and $\langle I_{out} \rangle_{min}$ are the maximum and minimum of the IVA for angles $0 \leq \rho < 90$. (The modulation efficiency that was calculated in our earlier publication²⁰ assumed a somewhat different functional form for P_{out} . See Section 6 for more details.) Using Equations 8, 10 and 11 it is straight forward to show that for a single HWP *and a single frequency*

$$P_{out}(\nu) = \frac{P_{in} \sin^2 \frac{\Delta\delta(\nu)}{2}}{1 + P_{in} \cos 2\alpha_{in} \cos^2 \frac{\Delta\delta(\nu)}{2}}, \quad (14)$$

and therefore

$$\epsilon(\nu) = \frac{P_{out}}{P_{in}} = \frac{\sin^2 \frac{\Delta\delta(\nu)}{2}}{1 + P_{in} \cos 2\alpha_{in} \cos^2 \frac{\Delta\delta(\nu)}{2}}. \quad (15)$$

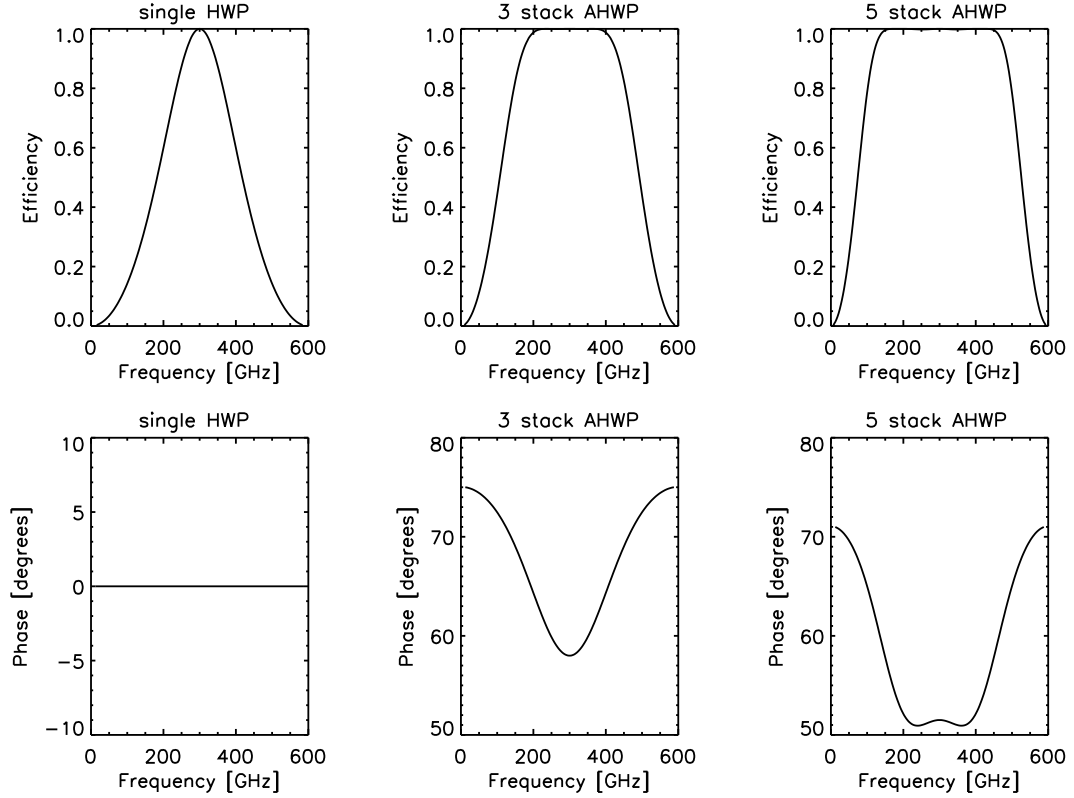


Fig. 3. Modulation efficiency $\epsilon = \epsilon(\nu, \Delta\nu = 0, \alpha_{in} = 0, \vec{\theta})$ (top) and the phase offset $\phi_0 = \phi(\alpha_{in} = 0, \nu, \Delta\nu = 0, \vec{\theta})$ (bottom) for the single HWP (left) and the three- (middle) and the five-stack (right) as a function of frequency.

There are two cases for which this expression is particularly useful, (i) when P_{in} is sufficiently small such that the denominator is approximately 1, and (ii) when $\alpha_{in} = 45$ degrees (for any level of P_{in}). In both of these cases

$$\epsilon(\nu) = \sin^2 \frac{\Delta\delta(\nu)}{2}, \quad (16)$$

ϵ is only a function of the retardance of the HWP and is independent of P_{in} . In the first case ϵ also does not depend on α_{in} .

We note that instead of using Equation 13 a more generally appropriate process for extracting the modulation efficiency is by fitting the IVA to a harmonic series of sine waves and then calculating

$$\epsilon = \frac{A_4}{A_0}, \quad (17)$$

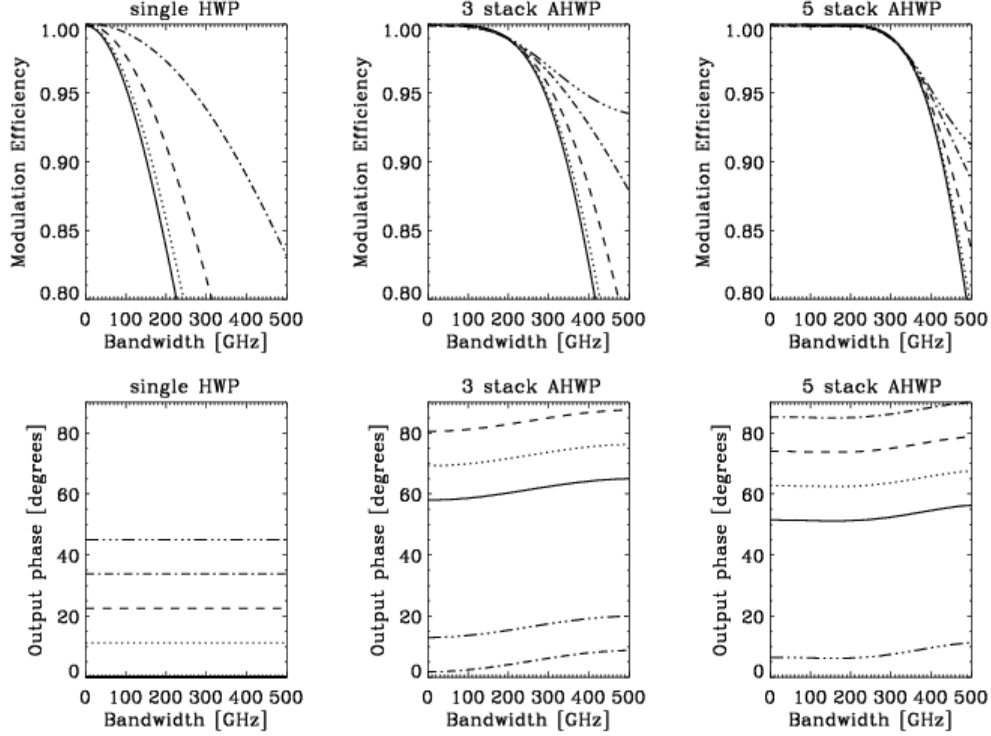


Fig. 4. Top: Modulation efficiency of the single HWP, the three- and the five-stack AHWPs as a function of detection bandwidth for input polarization angle of 0 (solid line), 22.5 (dot), 45 (dash), 67.5 (dot-dash), and 90 (three-dot dash) degrees. Bottom: Output phase angle of the single, three-, and five-stack as a function of detection bandwidth for the same input polarization angles as the top panels. For both the modulation efficiency and the phase, $\nu_c = \nu_{WHP}$.

where A_0 and A_4 are the coefficients of the zeroth and fourth harmonic terms, respectively. For the results presented in this paper there is no difference between the two processes.

The upper panels in Figure 3 give the modulation efficiency of a single HWP and of a three- and five-stack AHWP as a function of frequency. To calculate these efficiencies we analyzed monochromatic IVAs. The reduction in efficiency for the three-stack at a frequency of, for example, 150 GHz can be mapped to the smaller amplitude IVA in Figure 2 for the same frequency. The set of three panels shows that a larger number of plates in the stack gives a broader bandwidth of high modulation efficiency.

In order to reconstruct the polarization angle α_{in} of the incident polarization it is essential to examine the phase angle of the IVA. The lower panels in Figure 3 show ϕ_0 as a function of frequency. They were also extracted from IVAs calculated with monochromatic detection bandwidths. The phase offset varies with frequency even near the center frequency ν_{WHP} .

To gain some insight into the effects that we quantify in subsequent sections let us compare the middle panels of Figures 2 and 3 in more detail. The solid lines shown in Figure 2

were calculated for a center frequency of 150 GHz. The upper panel in Figure 2 shows the corresponding monochromatic IVA. The modulation efficiency of ~ 0.95 and phase angle of ~ 70 degrees of that IVA can be read directly from the middle panels of Figures 3 at a frequency of 150 GHz. The lower panel of Figure 2 shows an IVA that has been calculated for a detection bandwidth of ± 30 GHz around 150 GHz. It was calculated by averaging the intensities at different frequencies. We used a frequency resolution of 0.5 GHz (see Table 1). Each of these IVAs has a modulation efficiency and phase offset that can be read off from the middle panels of Figure 3. Both the modulation efficiency and the phase offset vary over the bandwidth. As a consequence, the resulting IVA is a superposition of sine waves with different amplitudes and phases. Hence the final IVA is also a sine wave, but its amplitude and phase depends on averaging intensities over frequencies.

In the next Section we discuss how the efficiency ϵ and the phase angle ϕ depend on the construction parameters of the stack of HWPs, on the center frequency, and on the detection bandwidth, and how to relate them to the parameters of the incident polarization P_{in} and α_{in} .

4. Reconstruction of P_{in} and α_{in}

4.A. Modulation Efficiency and Phase

The top panels of Figure 4 show the modulation efficiency of a single HWP, three-stack, and five-stack AHWPs as a function of bandwidth around $\nu_c = 300$ GHz. The different curves correspond to different input polarization angles α_{in} . To calculate the modulation efficiency we used $P_{in} = 1$. For $\alpha_{in} = 0$ degrees modulation efficiency that is larger than 0.99 is achieved with a bandwidth of 200 (300) GHz for the three (five)-stack AHWP, while a single HWP achieves a bandwidth of only 50 GHz. For a given bandwidth the modulation efficiency is a function of the orientation of the incident polarization α_{in} . So in order to reconstruct P_{in} , information about α_{in} needs to be extracted first from the measured phase angle ϕ .

The bottom panels of Figure 4 show the output phase angle ϕ as a function of bandwidth around $\nu_c = 300$ GHz. The phase of the single HWP shows flat response over the bandwidth. The phases of the IVA of the three- and five-stack AHWPs are a function of bandwidth, a result consistent with the bottom row of Figure 3. For a given bandwidth the phase angle ϕ has an overall offset ϕ_0 .

The conclusions so far are that if the incident radiation is known to be fully polarized and the detection bandwidth is known, then the orientation angle of the incident polarization and the modulation efficiency can be extracted. Alternatively, if the orientation angle of the incident fully polarized radiation is known then the modulation efficiency and an equivalent detection bandwidth can be extracted. These situations are encountered in the laboratory when calibrating the polarimeter.

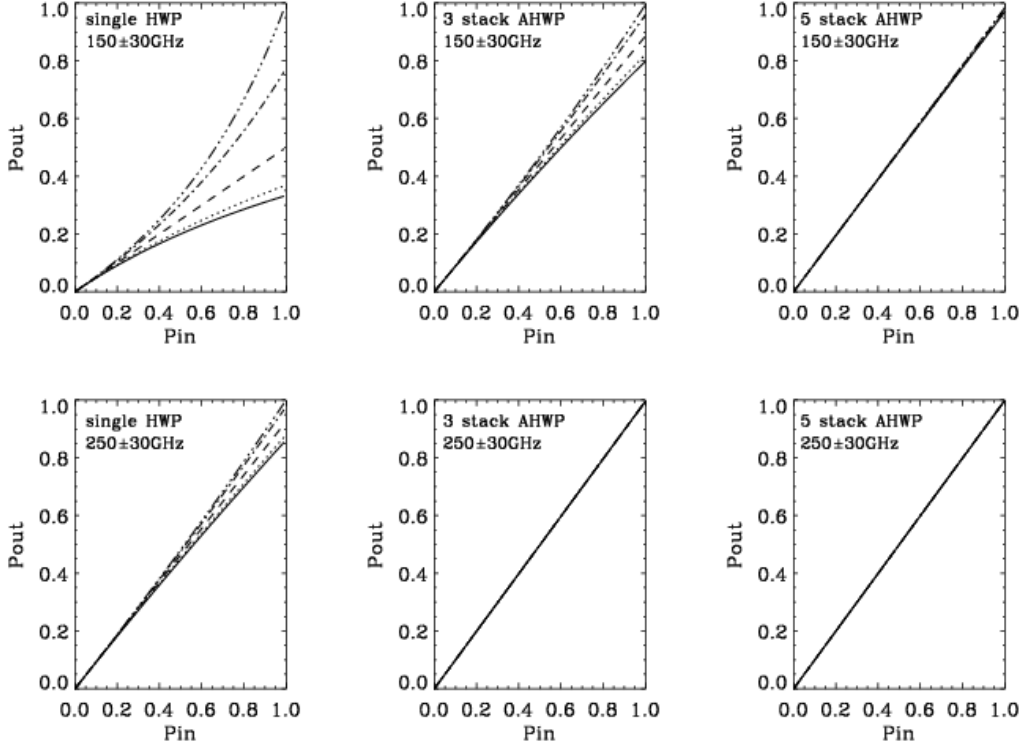


Fig. 5. The extracted degree of polarization P_{out} as a function of the degree of polarization of the incident light P_{in} for the single-, three-, and five-stack. Each curve corresponds to the input polarization angle of 0 (solid line), 22.5 (dot), 45 (dash), 67.5 (dot-dash), and 90 (three-dot dash) degrees. The frequency and the bandwidth are $\nu_c \pm \Delta\nu = 150 \pm 30$ GHz (top) and 250 ± 30 GHz (bottom). For all the panels, $\nu_{WP} = 300$ GHz.

4.B. P_{out} vs. P_{in}

The results in Figure 4 were calculated with the assumption of incident polarization $P_{in} = 1$. We relax this assumption in Figure 5, which shows P_{out} as a function of P_{in} for various angles α_{in} . The local slope of each curve is the modulation efficiency ϵ . The modulation efficiency is a function of both α_{in} and P_{in} . That this is the case for a single HWP is evident from Equation 15. In an actual observation both P_{in} and α_{in} are a-priori unknown, which suggests that reconstructing the polarimeter modulation efficiency, or the incident polarization P_{in} is subject to additional uncertainty. In many practical cases this is not a limitation for reasons that we now discuss.

Figure 5 shows that in cases where the incident polarization is known to be small the modulation efficiency is to a good approximation constant that does not depend either on P_{in} or on α_{in} (for the simple case of a single HWP see Equations 15 and 16). The region where the approximation 'small incident polarization' is valid depends on the construction parameters of the HWP and the detection bandwidth. For example, for the top middle and

$\epsilon_{45}^{+\epsilon_{max}} - \epsilon_{min}$	150 \pm 30 GHz	250 \pm 30 GHz
single HWP	0.50 $^{+0.055}_{-0.045}$	0.93 $^{+0.015}_{-0.015}$
three-stack AHWP	0.89 $^{+0.02}_{-0.02}$	0.996 $^{+0.001}_{-0.000}$
five-stack AHWP	0.976 $^{+0.002}_{-0.001}$	0.999 $^{+0.001}_{-0.000}$

Table 2. The modulation efficiency at $P_{in} = 0.1$ with $\alpha_{in} = 45$ degrees is shown. The modulation efficiency is calculated as a slope of $P_{out} - P_{in}$ relationship in Figure 5. The quoted errors are $\epsilon_{max} - \epsilon_{45}$ and $\epsilon_{min} - \epsilon_{45}$, where ϵ_{45} corresponds to the modulation efficiency at $\alpha_{in} = 45$ degrees at $P_{in} = 0.1$. The maximum and the minimum modulation efficiency corresponds to $\alpha_{in} = 90$ and 0 degrees, respectively.

bottom left panels the approximation is valid for $P_{in} \lesssim 0.2$. It is valid for a much larger range of P_{in} when using a 5-stack (see right panels), and even for the three-stack when it is used reasonably close to the designed band center (see middle bottom panel).

We note that the HWPs that are used for the calculations shown in Figure 5 are each designed for a center frequency of 300 GHz (see Table 1). Therefore the top left panel that shows the largest variation of the modulation efficiency with incidence angle is never likely to be used in practice. It describes a single HWP optimized for 300 GHz that is used for a band around 150 GHz. This panel is only shown for didactic purposes.

We find then that in many practical situations there is a unique relation between P_{in} and P_{out} , a relation that does not depend on the orientation angle of α_{in} . In the more general case when the value of P_{out} depends both on P_{in} and on α_{in} , the value of α_{in} needs to be determined first from the IVA. This is straight forward for a single HWP because the phase ϕ of the IVA is equal to $\alpha_{in}/2$ for any detection bandwidth; see for example the bottom left panel of Figure 4. The case of an AHWP is discussed in Section 4.C, but the conclusion is that for a specified bandwidth there is a unique relationship between the phase ϕ and the angle α_{in} . Therefore the procedure for finding P_{in} is to first determine α_{in} using the phase of the IVA and then use the relation between P_{out} and P_{in} that is appropriate for this α_{in} .

Laboratory measurements of modulation efficiency typically use incident polarizations that are close to $P_{in} = 1$ in order to increase the signal to noise ratio of the measurement. Figure 5 demonstrates that determinations of ϵ depend on the polarization angle α_{in} . An efficiency value that was determined in the laboratory using a particular angle α_{in} will not in general correspond to the modulation efficiency of the polarimeter during actual observations for which α_{in} is not known. A simple remedy is to align the incident polarization in the laboratory such that $\alpha_{in} = 45$ degrees. For that particular value the efficiency ϵ_{45} is a constant as a function of P_{in} and is equal to the same efficiency that would be measured with small incident polarizations. Table 2 summarizes this point in a quantitative way. The values shown give the efficiency expected with $\alpha_{in} = 45$ degrees for different frequency bands

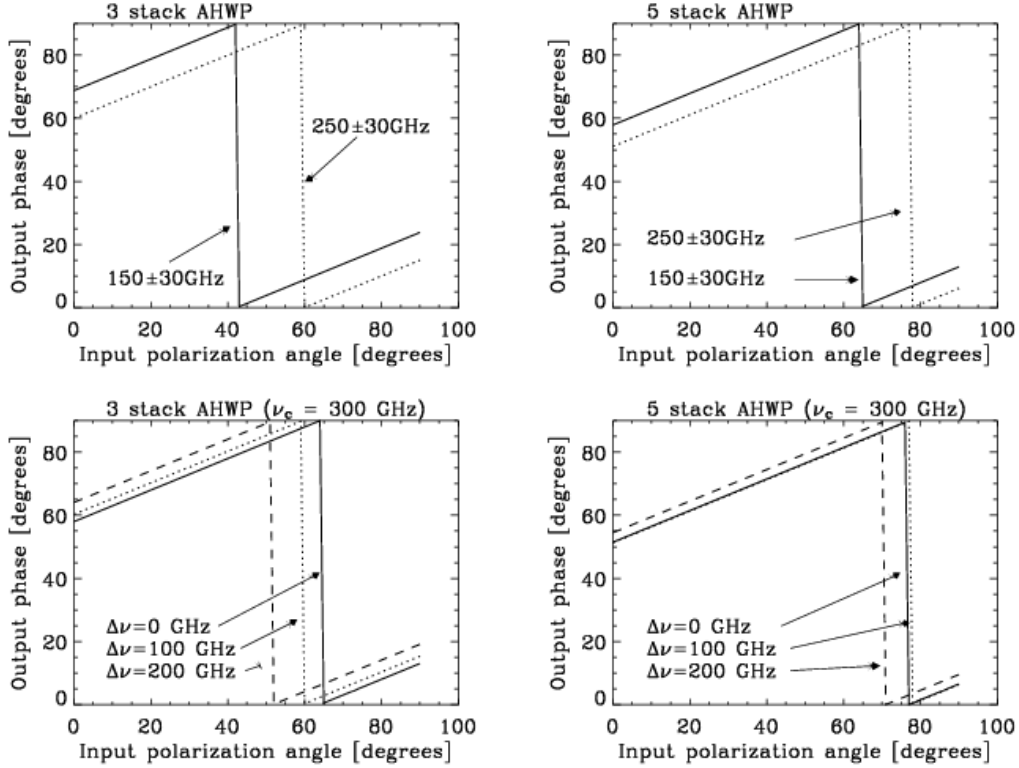


Fig. 6. The output phase angle of the three- (left) and the five-stack (right) AHPWs as a function of the input polarization angle. The top panels give results for 150 (solid) and 250 GHz (dot), each with a fixed bandwidth of ± 30 GHz. The bottom panels give results for a fixed center frequency of 300 GHz with bandwidths of ± 0 (solid), ± 100 (dot), and ± 200 (dash) GHz.

and for different HWP configurations. The upper and lower values marked with \pm give the additional increments of efficiency that would be determined if α_{in} was 90 (for plus) or 0 (for minus) degrees. For example, the modulation efficiency of a single HWP (that is constructed according to the parameters given in Table 1) at 150 GHz with a bandwidth of ± 30 GHz is 0.5 when measured with $\alpha_{in} = 45$ degrees. This value of ϵ does not depend on the magnitude of P_{in} . Yet for observations with $P_{in} = 0.1$ the modulation efficiency would be 0.055 (0.045) for $\alpha_{in} = 90$ (0) degrees. Whereas for the single HWP the variation in modulation efficiency could be as large as 10%, it is about 2% or smaller with the three- or five-stack. These values depend on the construction parameters of the HWP and on the detection bandwidth and thus can not be taken as general.

4.C. ϕ vs. α_{in}

In Section 4.B we investigated how the measured degree of polarization P_{out} relates to the input polarization P_{in} . We now quantify a similar relationship between ϕ and α_{in} . Figure 6

shows the phase angle as a function of the input polarization angle for the three- and five-stack AHWPs. (Recall that ϕ is a constant over frequency for a single HWP, see the bottom left panel of Figure 4.) The panels show that α_{in} and ϕ have a linear relationship with a slope of 0.5, and that this slope does not depend on the construction parameters of the HWP nor on the detection bandwidth. However, the phase offset *is* a function of ν_c and $\Delta\nu$.

The magnitude of the phase offset ϕ_0 is a critical parameter in the reconstruction of an unknown incident polarization angle α_{in} . Since this phase offset is a function of the spectral response of the instrument it can either be calculated, if the spectral response is known, or measured in the laboratory by varying α_{in} of a known source and extracting ϕ from the IVA. (See however Section 5 for important caveats.) Errors in this calibration will propagate to errors in the determination of α_{in} for a source whose polarization properties are not known.

The direction of rotation of the AHWP affects the relationship between ϕ and α_{in} . With single HWP $\phi = \pm\alpha_{in}/2$, where the sign is determined by the direction of rotation. For our particular choice of directions (see Figure 1) we have $\phi = +\alpha_{in}/2$. However, the orientation angles of the stack of plates break the rotational symmetry for an AHWP and in general there are four possible choices

$$\phi = \pm\frac{1}{2}\alpha_{in} + \phi_0, \quad (18)$$

$$\phi = \pm\frac{1}{2}\alpha_{in} + \frac{\pi}{2} - \phi_0. \quad (19)$$

In Equation 19 the phase offset is no longer ϕ_0 , but $\frac{\pi}{2} - \phi_0$. For our particular choice, where both ρ and the AHWP orientation angles $\vec{\theta}$ are counterclockwise in the xy plane (as shown in Figure 1), Equation 18 with a plus sign gives the relevant functional dependence.

5. Spectrum of Incident Radiation

So far we assumed an incident radiation spectrum that was constant with frequency. We now address the more general case where the spectrum of the incident radiation is a function of frequency. In this case the phase offset ϕ_0 depends on the details of this spectrum. Since ϕ_0 is required for reconstruction of P_{in} and α_{in} , the consequence is that knowledge of the incident spectrum is also required.

To assess this effect quantitatively we consider three distinct spectra: (1) black body with the temperature of the cosmic microwave background radiation, (2) black body with a temperature of 300 K, and (3) galactic dust. We choose these spectra because they are relevant for calibration and for measurements of the polarization of the CMB at frequencies between 100 and 500 GHz. We assume the following spectra $I(\nu)$,

$$I_{CMB}(\nu) = B(T_{CMB}, \nu), \quad (20)$$

$$I_{dust}(\nu) = A\nu^\gamma B(T_{dust}, \nu), \quad (21)$$

	CMB	Dust	Lab
150 \pm 30 GHz	$\phi_0 = 57.86$	56.69	57.33
250 \pm 30 GHz	51.12	51.16	51.14
420 \pm 30 GHz	53.85	54.50	54.49

	CMB – Dust	CMB – Lab	Dust – Lab
150 \pm 30 GHz	$\Delta\phi = 1.17$ ($\Delta\alpha_{in} = 2.34$)	0.53 (1.06)	-0.64 (-1.28)
250 \pm 30 GHz	-0.04 (-0.08)	-0.02 (-0.04)	0.02 (0.04)
420 \pm 30 GHz	-0.65 (-1.3)	-0.64 (-1.28)	0.01 (0.02)

Table 3. Top: The offset angles with four different spectra are shown. Bottom: The difference of the offset phase between different spectra. The number in a parenthesis is the difference in terms of the polarization angle α_{in} on the sky. A unit of the phase is in degrees.

$$I_{lab}(\nu) = B(T_{lab}, \nu), \quad (22)$$

$$B(T, \nu) = \frac{2\pi h}{c^2} \frac{\nu^3}{e^{\frac{h\nu}{k_B T}} - 1}, \quad (23)$$

where B denotes a black body spectrum, $T_{CMB} = 2.73$ K, $A = 4 \times 10^{-7}$, $\gamma = 1.75$, $T_{dust} = 18$ K, and $T_{lab} = 300$ K. We assume that the fractional polarization and the polarization angle of the incident radiation do not depend on frequency. We also assume that the degree of linear polarization of the CMB, of the galactic dust, and of a 300 K black body source are $P_{CMB} = 1 \times 10^{-6}$, $P_{dust} = 0.1$, and $P_{lab} = 1$, respectively.

The calculated phase offsets of a five-stack AHWP are summarized in Table 3. The top table shows the phase offset in unit of degrees. The bottom table shows the difference of the phase offsets between the different spectra. The parentheses indicate the level of difference in terms of polarization angle α_{in} .

Assume that a 300 K source is used in the laboratory to calibrate the phase offset and that the laboratory measurement agrees with the phase offsets given in the right hand column of the top part of Table 3. If these values are used for either CMB or dust observations, they would give rise to errors in position angle of the polarization on the sky as given in parentheses in the two right columns of the bottom table. The correct prescription is to validate the design of the instrument using the laboratory measurements and then use the predicted phase offsets given assumptions or measurements of the spectra of the sources. An uncertainty in the knowledge of the spectrum would give an uncertainty in the determination of α_{in} . The designer of a polarimeter with an AHWP should plan for this uncertainty and its mitigation during the analysis of the data.

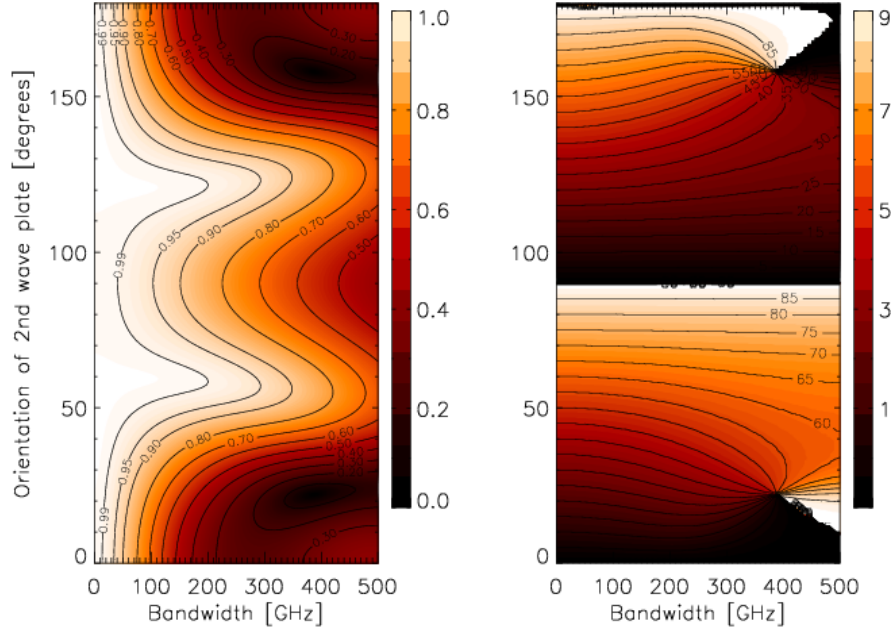


Fig. 7. The modulation efficiency (left) and the phase offset (right) of the three-stack AHWP as a function of the angle of the second plate θ_2 and the bandwidth $\Delta\nu$ around a center frequency of $\nu_{WP} = 300$ GHz. The color scale of the phase offset is in units of degrees. In both plots, the input polarization angle is $\alpha_{in} = 0$.

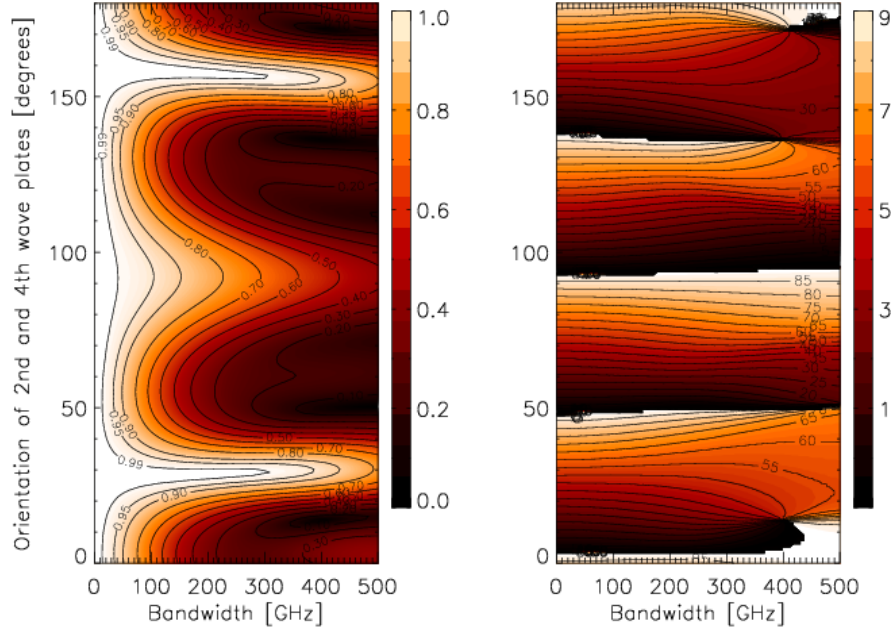


Fig. 8. The modulation efficiency (left) and the phase offset (right) of the five-stack AHWP as a function of the orientation angles of the second and fourth plates. The other angles are fixed at the values given in Table 1.

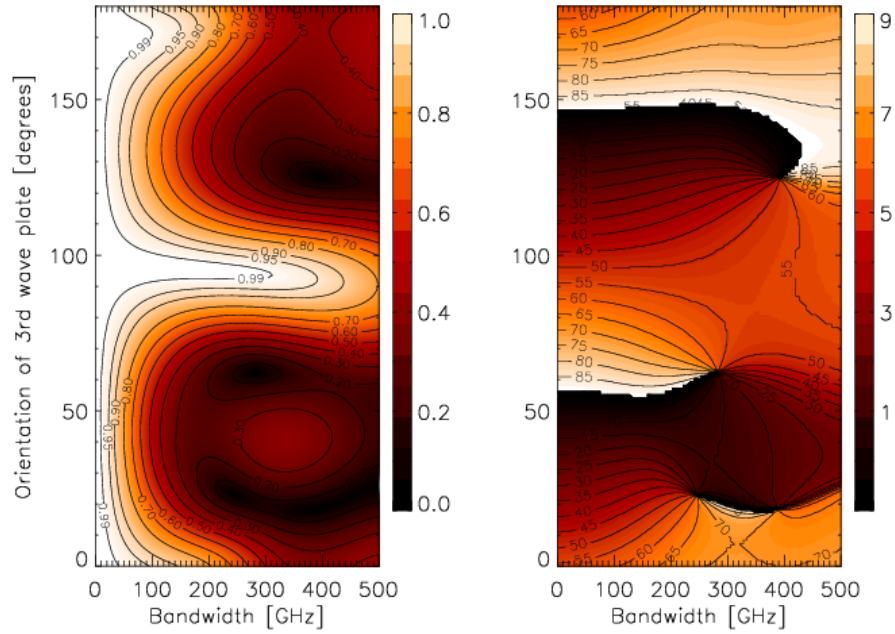


Fig. 9. The modulation efficiency (left) and the phase offset (right) of the five-stack AHPW as a function of the orientation angle of the third plate. The other angles are fixed at the values given in Table 1.

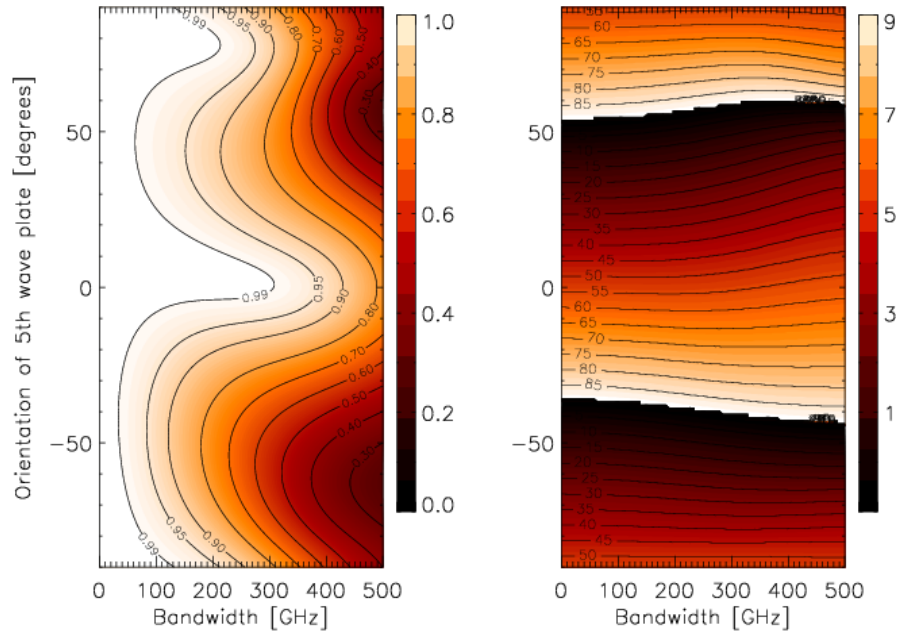


Fig. 10. The modulation efficiency (left) and the phase offset (right) of the five-stack AHPW as a function of the orientation angle of the fifth plate. The other angles are fixed at the values given in Table 1.

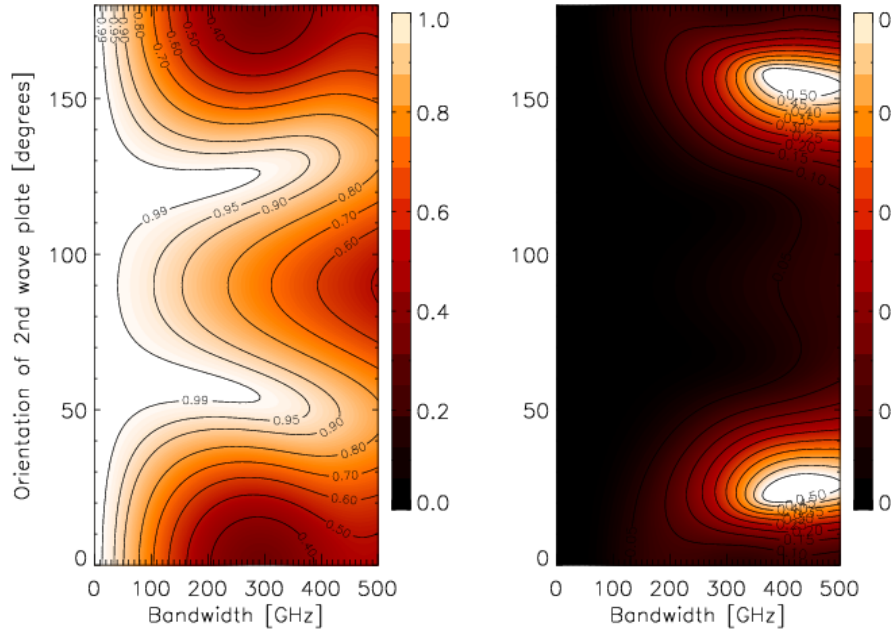


Fig. 11. The modulation efficiency of a three-stack AHWP based on Equation 24 (left) and the difference between this efficiency and the one calculated in Figure. 11 (right).

6. AHWP Performance vs. orientation angles $\vec{\theta}$

We have already pointed out in an earlier publication that it is relatively easy to achieve a high modulation efficiency with the three and five-stacks in terms of the requirements on the relative orientation of the plates.²⁰ In this section we expand on our earlier work and give a more thorough discussion. All of the analysis in this section assume a constant spectrum for the incident radiation.

The left panels of Figures 7, 8, 9, and 10 give contour plots for the modulation efficiency as a function of the orientation of the plates in the stacks. The modulation efficiency is calculated based on Equation 13 with Equations 7 and 12. The right panels of the same figures show the phase offset as defined in Equation 9.

For a three-stack Title¹⁸ showed that the highest modulation efficiency is achieved with a set of angle $\vec{\theta} = (0, 58, 0)$. The left panel of Figure 7 shows that this modulation is a weak function of the orientation of the middle plate near peak efficiency. The right panel of Figure 7 shows that for a second plate orientation $80 \lesssim \theta_2 \lesssim 100$ degrees the phase offset ϕ_0 is essentially independent of detection bandwidth. This orientation angle, however, does not give the broadest range of frequencies for high modulation efficiency. On the other hand, with an angle of 58 degrees, which gives the broadest range of modulation efficiency, the phase offset has stronger dependence on the detection bandwidth. Experiment designers need to consider this trade-off between bandwidth for high modulation and for constant phase offset.

The three-stack has zero modulation efficiency at θ_2 close to 20 and 160 degrees and detection bandwidth of 400 GHz. This is because there is a strong variation of the phase offset angle ϕ_0 with frequency near these parameters. Therefore, these points in the parameter space give the resultant IVA zero modulation amplitude, and correspondingly no phase can be defined as demonstrated by the singularities in the phase offset panel. The color discontinuity extending from the phase offset singularity toward bottom right is a consequence of phase offset periodicity. It is neither an artifact nor a real discontinuity. Phases that are larger than 90 degrees are interpreted as positive values close to zero. Similar features appear in Figures 8, 9, and 10.

With the five-stack, achieving high modulation efficiency requires higher accuracy of alignment of the second, third, and fourth wave plates than that required in the case of the three-stack. Little accuracy is required from the orientation of the fifth plate in the five-stack. The efficiency is most sensitive to the orientation of the second and fourth plates, and an accuracy of 5 degrees is required to maintain efficiency higher than 0.95 over 300 ± 150 GHz.

In a previous publication²⁰ we gave results for the modulation efficiency that was based on the following expression

$$P_{out} = \left\langle \frac{I_{max} - I_{min}}{I_{max} + I_{min}} \right\rangle, \quad (24)$$

which is different from the more correct definition given in Equation 13. The left panel of Figure 11 is the modulation efficiency based on Equation 24 with the same parameters that produced Figure 7. The right panel shows the differences between the two results. The modulation efficiency in Figure 7 accounts for the phase variation of the IVA curves as a function of frequency. In contrast the modulation efficiency in Figure 11 does not encode this variation.

7. Discussion

We analyzed the performance of a three- and five-stack AHWP polarimeters operating in the sub-millimeter wave band. Let us summarize the points that have been discussed and make some additional comments where appropriate.

- Three- and five-stack AHWP polarimeters provide broad bandwidth with high modulation efficiency.
- Their IVA has a phase offset that depends on the construction parameters of the stack, on the spectral response of the instrument, and on the spectrum of incident radiation. (our discussion assumed that the degree of polarization and the angle were independent of frequency with the detection bandwidth.)
- If the spectral response of the instrument, and the spectrum of the source are known,

then measurements of the phase of the IVA can give the orientation angle of the incident polarization.

We note that in many cases much of the radiation incident on the detector is due to emission by the telescope itself. If this emission is polarized it too will affect the phase of the IVA and hence the measurement of the angle of incident polarization.

- measurement uncertainties in either the spectral response of the instrument or the spectrum of the source translate to uncertainties in the reconstruction of the angle of incident polarization. The amount of uncertainty needs to be assessed on a case-by-case basis.
- Measurements of the amplitude of the IVA, which gives the degree of output polarization, can be uniquely inverted, in most cases, to give the input polarization if the modulation efficiency is known.
- In some cases information about the angle of the incident polarization needs to be used together with the modulation efficiency to find the incident degree of polarization.
- Laboratory measurement to find the modulation efficiency that are conducted with a source that has high degree of polarization should have an incident polarization angle of 45 degrees. At this angle the measured efficiency is the same as would be measured at any angle when P_{in} is small.
- We discussed how the modulation efficiency and phase offset of the polarimeters depend on errors in the orientation of the plates. Generally, an accuracy of few degrees is sufficient to ensure close the ideal performance.
- We discussed the how the incident spectrum of the radiation affects the IVA and the extraction of the parameters of the incident radiation.

Our analysis assumed a spectral response of the instrument that was top-hat in shape over a range in frequencies. This is an idealization. In any practical instrument, the entire spectral response of the instrument is necessary in order to reconstruct the parameters of the incident polarization.

References

1. J. M. Kovac, E. M. Leitch, C. Pryke, J. E. Carlstrom, N. W. Halverson, and W. L. Holzapfel. Detection of polarization in the cosmic microwave background using DASI. *Nature*, 420:772, December 2002. astro-ph/0209478.

2. L. Page, G. Hinshaw, E. Komatsu, M. R. Nolta, D. N. Spergel, C. L. Bennett, C. Barnes, R. Bean, O. Dore, M. Halpern, R. S. Hill, N. Jarosik, A. Kogut, M. Limon, S. S. Meyers, N. Odegard, H. V. Peiris, G. S. Tucker, L. Verde, J. L. Weiland, E. Wollack, and E. L. Wright. Three Year Wilkinson Microwave Anisotropy Probe (WMAP) Observations: Polarization Analysis. *ApJ* submitted, March 2006. astro-ph/0603450.
3. P. Oxley, P. Ade, C. Baccigalupi, P. deBernardis, H.-M. Cho, M. J. Devlin, S. Hanany, B. R. Johnson, T. Jones, A. T. Lee, T. Matsumura, A. D. Miller, M. Milligan, T. Renbarger, H. G. Spieler, R. Stompoer, G. S. Tucker, and M. Zaldarriaga. The EBEX Experiment. In W. L. Barnes and J. J. Butler, editors, *Earth Observing Systems IX: Infrared Spaceborne Remote Sensing*, volume 5543 of *Proceedings of SPIE*, pages 320331, 2004. astro-ph/0501111.
4. J. Kovac, BICEP/SPUD collaboration. Bicep2 and spud: Searching for inflation with degree-scale polarimetry from the south pole. 2007 AAS/AAPT Joint Meeting, American Astronomical Society Meeting 209, *Bulletin of the American Astronomical Society*, 38, 2007.
5. A. C. Taylor, A. Challinor, D. Goldie, K. Grainge, M. E. Jones, A. N. Lasenby, S. Withington, G. Yassin, W. K. Gear, L. Piccirilo, P. Ade, P. D. Mauskopf, B. Maei, and G. Pisano. Clover - a new instrument for measuring the b-mode polarization of the cmb. In *Proceedings of the XXXVIXth Rencontres de Moriond Exploring the Universe*, 2004.
6. <http://quiet.uchicago.edu/>
7. T. E. Montroy, P. A. R. Ade, R. Bihary, J. J. Bock, J. R. Bond, J. Brevick, C. R. Contaldi, B. P. Crill, A. Crites, O. Dor, L. Duband, S. R. Golwala, M. Halpern, G. Hilton, W. Holmes, V. V. Hristov, K. Irwin, W. C. Jones, C. L. Kuo, A. E. Lange, C. J. MacTavish, P. Mason, J. Mulder, C. B. Nettereld, E. Pascale, J. E. Ruhl, A. Trangsrud, C. Tucker, A. Turner, M. Viero. Spider: a new balloon-borne experiment to measure cmb polarization on large angular scales. *Proceedings of the SPIE*, 6267, 2006.
8. A. Kogut, D.T. Chuss, D. Fixsen, G.F. Hinshaw, M. Limon, S.H. Moseley, N. Phillips, E. Sharp, E.J. Wollack, K. U-Yen. Pappa: Primordial anisotropy polarization pathfinder array. *J. Opt. Soc. Am.*, 69, 1979.
9. <http://bolo.berkeley.edu/polarbear/>
10. T. J. Jones and D. I. Klebe. A simple infrared polarimeter. *PASP*, 100:11581161, September 1988.
11. S. R. Platt, R. H. Hildebrand, R. J. Pernic, J. A. Davidson, and G. Novak. 100-micron array polarimetry from the Kuiper Airborne Observatory - Instrumentation, techniques, and first results. *PASP*, 103:11931210, November 1991.
12. R. W. Leach, D. P. Clemens, B. D. Kane, and R. Barvainis. Polarimetric mapping of Orion using MILLIPOL - Magnetic activity in BN/KL. *Astrophys. J.*, 370:257262, 23

March 1991.

13. A. G. Murray, R. Nartallo, C. V. Haynes, F. Gannaway, and P. A. R. Ade. An Imaging Polarimeter for SCUBA. In ESA SP-401: The Far Infrared and Submillimetre Universe, pages 405+, 1997.
14. B.R.Johnson, J.Collins, M.E.Abroe, P.A.R.Ade, J.Bock, J.Borrill, A.Boscaleri, P.de Bernardis, S.Hanany, A.H. Jae, T.Jones, A.T.Lee, L.Levinson, T.Matsumura, B.Rabii, T.Renbarger, P.L.Richards, G.F.Smoot, R.Stompor, H.T.Tran, C.D.Winant, J.H.P.Wu, J.Zuntz. Maxipol: Cosmic microwave background polarimetry using a rotating half-wave plate. astro-ph/0611394, 2006.
15. J. H. P. Wu, J. Zuntz, M. E. Abroe, P. A. R. Ade, J. Bock, J. Borrill, J. Collins, S. Hanany, A. H. Jae, B. R. Johnson, T. Jones, A. T. Lee, T. Matsumura, B. Rabii, T. Renbarger, P. L. Richards, G. F. Smoot, R. Stompor, H. T. Tran, C. D. Winant. Maxipol: Data analysis and results. astro-ph/0611392, 2006.
16. S. Pancharatnam. Achromatic combinations of birefringent plates. Raman Research Inst. Bangalore, Memoir, 71:137144, 1955.
17. A. M. Title. Improvement of birefringent lters. Applied Optics, 14:229237, 1975.
18. A. M. Title and W. J. Rosenberg. Achromatic retardation plates. In Polarizers and Applications, SPIE Proceedings Vol. 307. Edited by Giorgio B. Trapani. Bellingham, WA: Society for Photo-Optical Instrumentation Engineers, 1981., p.120, January 1981.
19. J. Tinbergen. Astronomical Polarimetry. Cambridge University Press, Cambridge, UK, 1996.
20. S. Hanany, H. Hubmayr, B. R. Johnson, T. Matsumura, P. Oxley, and Thibodeau M. Millimeter-wave achromatic half-wave plate. Applied Optics, 44:46664670, August 2005.
21. E. V. Loewenstein. Optical Constants for Far Infrared Materials. I. Crystalline Solids. Applied Optics, 12(2):398406, February 1973.

List of Figure Captions

Fig. 1. A schematic diagram of the HWP polarimeter model. The transmission axis of a linear polarizer is parallel to the x axis.

Fig. 2. IVA for monochromatic light (top panels) and for broadband radiation (bottom panels) for a single HWP, a three-stack AHWP, and a five-stack AHWP (left to right). See Table 1 for the parameters of the plates and for the details about the simulations used for the calculations. Frequencies of 150 (solid), 200 (dash), 250 (dot), 300 (dash-dot) GHz are used for the case of monochromatic light. For the broadband case we use 150 ± 30 GHz (solid) and 250 ± 30 GHz (dot). In all the panels, the maximum intensity is normalized to 1.

Fig. 3. Modulation efficiency $\epsilon = \epsilon(\nu, \Delta\nu = 0, \alpha_{in} = 0, \vec{\theta})$ (top) and the phase offset $\phi_0 = \phi(\alpha_{in} = 0, \nu, \Delta\nu = 0, \vec{\theta})$ (bottom) for the single HWP (left) and the three- (middle) and the five-stack (right) as a function of frequency.

Fig. 4. Top: Modulation efficiency of the single HWP, the three- and the five-stack AHWPs as a function of detection bandwidth for input polarization angle of 0 (solid line), 22.5 (dot), 45 (dash), 67.5 (dot-dash), and 90 (three-dot dash) degrees. Bottom: Output phase angle of the single, three-, and five-stack as a function of detection bandwidth for the same input polarization angles as the top panels. For both the modulation efficiency and the phase, $\nu_c = \nu_{WHP}$.

Fig. 5. The extracted degree of polarization P_{out} as a function of the degree of polarization of the incident light P_{in} for the single-, three-, and five-stack. Each curve corresponds to the input polarization angle of 0 (solid line), 22.5 (dot), 45 (dash), 67.5 (dot-dash), and 90 (three-dot dash) degrees. The frequency and the bandwidth are $\nu_c \pm \Delta\nu = 150 \pm 30$ GHz (top) and 250 ± 30 GHz (bottom). For all the panels, $\nu_{WHP} = 300$ GHz.

Fig. 6. The output phase angle of the three- (left) and the five-stack (right) AHWPs as a function of the input polarization angle. The top panels give results for 150 (solid) and 250 GHz (dot), each with a fixed bandwidth of ± 30 GHz. The bottom panels give results for a fixed center frequency of 300 GHz with bandwidths of ± 0 (solid), ± 100 (dot), and ± 200 (dash) GHz.

Fig. 7. The modulation efficiency (left) and the phase offset (right) of the three-stack AHWP as a function of the angle of the second plate θ_2 and the bandwidth $\Delta\nu$ around a center frequency of $\nu_{WHP} = 300$ GHz. The color scale of the phase offset is in units of degrees. In both plots, the input polarization angle is $\alpha_{in} = 0$.

Fig. 8. The modulation efficiency (left) and the phase offset (right) of the five-stack AHWP as a function of the orientation angles of the second and fourth plates. The other angles are fixed at the values given in Table 1.

Fig. 9. The modulation efficiency (left) and the phase offset (right) of the five-stack AHWP as a function of the orientation angle of the third plate. The other angles are fixed at the

values given in Table 1.

Fig. 10. The modulation efficiency (left) and the phase offset (right) of the five-stack AHWP as a function of the orientation angle of the fifth plate. The other angles are fixed at the values given in Table 1.

Fig. 11. The modulation efficiency of a three-stack AHWP based on Equation 24 (left) and the difference between this efficiency and the one calculated in Figure. 11 (right).

Table Caption

Tab. 1. Parameters of the wave plates and parameters used in the simulations to calculate the IVA.

Tab. 2. The modulation efficiency at $P_{in} = 0.1$ with $\alpha_{in} = 45$ degrees is shown. The modulation efficiency is calculated as a slope of $P_{out} - P_{in}$ relationship in Figure 5. The quoted errors are $\epsilon_{max} - \epsilon_{45}$ and $\epsilon_{min} - \epsilon_{45}$, where ϵ_{45} corresponds to the modulation efficiency at $\alpha_{in} = 45$ degrees at $P_{in} = 0.1$. The maximum and the minimum modulation efficiency corresponds to $\alpha_{in} = 90$ and 0 degrees, respectively.

Tab. 3. Top: The offset angles with four different spectra are shown. Bottom: The difference of the offset phase between different spectra. The number in a parenthesis is the difference in terms of the polarization angle α_{in} on the sky. A unit of the phase is in degrees.